Available online at www.sciencedirect.com

ScienceDirect

Geochimica et Cosmochimica Acta 265 (2019) 313–329

Geochimica et Cosmochimica Acta

www.elsevier.com/locate/gca

An experimental study of the solubility and speciation of tungsten in NaCl-bearing aqueous solutions at 250, 300, and 350 °C

Xin-Song Wang [a,b,*], Alexander Timofeev [b], A.E. Williams-Jones [b], Lin-Bo Shang [a], Xian-Wu Bi [a,*]

[a] State Key Laboratory of Ore Deposits Geochemistry, Institute of Geochemistry, Chinese Academy of Sciences, Guiyang 550002, China
[b] Department of Earth & Planetary Sciences, McGill University, 3450 University Street, Montreal, QC H3A 0E8, Canada

Received 20 April 2019; accepted in revised form 6 September 2019; available online 16 September 2019

Abstract

The solubility of tungsten trioxide solid and the speciation of tungsten in NaCl-bearing solutions have been investigated through experiments conducted at 250, 300, and 350 °C under vapour-saturated water pressure. Based on the results of these experiments, the solubility of tungsten trioxide was controlled by temperature and pH, whereas the NaCl concentration did not affect the solubility except through its influence on the ionic strength of the solution. Two tungsten species were found to be present in the solutions, namely $H_2WO_4^0$ at low pH and HWO_4^- at higher pH. These two species formed via the reactions $WO_3 + H_2O = H_2WO_4^0$ and $WO_3 + H_2O = HWO_4^- + H^+$, respectively. The logarithms of the equilibrium constants for these reactions are -5.18 ± 0.26, -4.97 ± 0.25, -4.69 ± 0.10, and -7.91 ± 0.30, -7.67 ± 0.29, -7.52 ± 0.18 for 250, 300, and 350 °C, respectively. In addition, the logarithms of the first and second association constants of $H_2WO_4^0$ were determined to be 2.72, 2.71, 2.83, and 5.59, 6.49, 8.07 for 250, 300, and 350 °C, respectively. These values indicate that $H_2WO_4^0$ is only important at low pH values (<2.8), and that HWO_4^- is the dominant tungsten species at pH conditions commonly encountered in nature. The data obtained in this study were used to model the solubility of scheelite and ferberite. This modeling indicates that tungsten concentrations are highest at high temperature in solutions with high salinity, low contents of calcium and iron, and either very low or high pH. The opposite is true for tungsten mineral precipitation from a fluid.

Keywords: Tungsten solubility and speciation; Tungsten mineralization; Hydrothermal systems; Formation constants

1. INTRODUCTION

Numerous studies have shown that economic tungsten deposits (dominantly greisen and quartz-vein type in which wolframite and/or scheelite are the ore minerals) form from NaCl-dominated brines (3–12 wt.% NaCl) at temperatures in the range 200–400 °C (Campbell and Robinsoncook, 1987; Polya, 1989; Bailly et al., 2002; Lu et al., 2003; Romer and Lüders, 2006; Wei et al., 2012; Ni et al., 2015; Zhu and Peng, 2015; Lecumberri-Sanchez et al., 2017; Soloviev and Kryazhev, 2017; Korges et al., 2018). Most of these studies have also proposed models for the formation of the ores, e.g., fluid mixing, cooling, boiling, and fluid-rock interaction (Campbell et al., 1984; Polya, 1988; Bailly et al., 2002; Lu et al., 2003; Ni et al., 2015; Lecumberri-Sanchez et al., 2017; Korges et al., 2018). In

* Corresponding authors at: State Key Laboratory of Ore Deposits Geochemistry, Institute of Geochemistry, Chinese Academy of Sciences, Guiyang 550002, China (X.-S. Wang and X.-W. Bi).

E-mail addresses: wangxinsong@mail.gyig.ac.cn (X.-S. Wang), bixianwu@vip.gyig.ac.cn (X.-W. Bi).

https://doi.org/10.1016/j.gca.2019.09.013
0016-7037/

order, however, to reliably model tungsten ore formation, the speciation of tungsten at elevated temperature needs to be known, and thermodynamic data are needed for the dominant species. Unfortunately, there is little agreement on the nature of the main tungsten species at elevated temperature and only a small number of studies have reported robust thermodynamic data for aqueous tungsten species based on experiments.

Although most researchers consider that tungsten occurs dominantly as tungstate species in hydrothermal fluids and therefore forms ion pairs with cations like H^+, Na^+ and K^+ (Wesolowski et al., 1984; Wood and Vlassopoulos, 1989; Wood, 1992; Wood and Samson, 2000), some researchers have proposed that it also occurs as complexes involving anions, particularly Cl^- (Manning and Henderson, 1984). Thus, for example, Manning and Henderson (1984) proposed that WCl_6, $WOCl_4$ or $(WO_3)_2Cl^-$, are the dominant tungsten species in brines at magmatic conditions. Keppler and Wyllie (1991) reached exactly the opposite conclusion, namely that halogen complexes are not involved in tungsten dissolution at these conditions. Wood and Vlassopoulos (1989) and Wood (1992) evaluated the proposed role of chloride species in the aqueous mobilization of tungsten experimentally by investigating the solubility of WO_3 in HCl-bearing solutions at 500 °C and 300–600 °C, respectively. They showed convincingly that Cl^- complexes do not play a role in tungsten transport and, instead, that $H_2WO_4^0$ is the dominant tungsten species in HCl-bearing solutions, at least under acidic conditions; they reported equilibrium constants for the corresponding dissolution reaction. In an earlier potentiometric study and temperatures up to 300 °C, Wesolowski et al. (1984) showed that at higher pH, $H_2WO_4^0$ gives way to HWO_4^- and HWO_4^- gives way, in turn, to WO_4^{2-} as the dominant tungsten species. Because of the importance of NaCl-dominated brines in the transport of tungsten in ore-forming hydrothermal systems, some researchers have proposed that the tungstate ion may form stable ion pairs with Na^+. Indeed, this was the conclusion reached by Wood and Vlassopoulos (1989) from the observation that the solubility of WO_3 increases with increasing NaCl and NaOH contents of aqueous solutions. Because of the lack of a dependence of this solubility on pH, they also concluded that this ion pair is $NaHWO_4^0$ and reported an equilibrium constant for the corresponding dissolution reaction. Gibert et al. (1992) re-evaluated the data of Wood and Vlassopoulos (1989) and showed that they could be explained without invoking ion pairs involving Na^+. Wood and Samson (2000), subsequently argued that, because of the increased electrostatic attraction among ions at high temperature due to the decreased dielectric constant of water, it is highly probable that the neutral ion pair, $NaHWO_4^0$, dominates tungsten transport in hydrothermal systems. Recent molecular dynamic simulations for Cu(I), Au(I), and Zn(II) complexes, however, challenge this conclusion by demonstrating that charged species can predominate in high density fluids, even at high temperature (Mei et al., 2014, 2015). In summary, although it has been clearly established that tungstate forms stable species with H^+, it is not clear whether or not tungstate also forms stable species with Na^+. In view of this and the importance of NaCl-dominant brines in transporting tungsten in ore-forming systems involving this metal, it is essential that the question of the stability of Na^+-tungstate ion pairs be resolved, especially for the temperatures of tungsten ore-formation (200–400 °C).

In this paper, we report results of experiments designed to evaluate tungsten solubility and speciation in the system H_2O-NaCl at temperatures of 250, 300, and 350 °C. These results show that, in solutions containing up to 4 m NaCl (18.9 wt.% NaCl), tungstic acid ($H_2WO_4^0$) is the dominant tungsten species at low pH and HWO_4^- is the dominant species at mildly acidic to near-neutral conditions. Although the solubility of tungsten (WO_3) increases with increasing NaCl content of the solution, this is due to the resulting increase in the ionic strength of the solution and not the formation of tungstate ion pairs with Na^+. We close the paper by retrieving thermodynamic data for $H_2WO_4^0$ and HWO_4^- and using them to model and evaluate mechanisms for the transport of tungsten and the precipitation of scheelite and wolframite in a hydrothermal fluid.

2. METHODS

2.1. Experiments

The experimental equipment and methods adopted in this study are the same as those used in previous studies at McGill University (Migdisov and Williams-Jones, 2007; Timofeev et al., 2017). The experiments were carried out in batch-type titanium grade 2 autoclaves, which were heated in a Fisher Isotemp oven equipped with a stainless-steel box to reduce thermal gradients. Prior to each experiment, the autoclaves were cleaned by filling them with 7 wt.% nitric acid (Trace metal grade) for 12 h, then twice with 3 wt.% ammonia hydroxide (Trace metal grade) for 6 h, and finally with nano-pure water for 24 h. This treatment ensured that no tungsten from previous experiments remained on the walls of the autoclaves.

The solubility of tungsten (VI) trioxide solid was investigated in aqueous solutions of variable NaCl concentration and pH at temperatures of 250, 300, and 350 °C, and vapor-saturated water pressure. The sodium chloride solutions were prepared to have concentrations ranging from 0.0005 mol/L to 4.0 mol/L; the pH of the solutions was varied by adding small amounts of HCl and ranged from 1.12 to 2.97 at ambient temperature. Solid reactant (WO_3, yellow powder; Alfa Aesar 99.998% purity) was introduced into a small quartz holder (~3.5 cm long) that was then capped by quartz wool to prevent mechanical transfer of the solid to the solution. In order to ensure that the experiments were conducted at conditions for which the tungsten would be in the 6+ state, the oxygen fugacity of the solutions was buffered by MoO_3 (light yellow powder; Alfa Aesar 99.95% purity) and MoO_2 (brown powder; Alfa Aesar, 99% purity), which were introduced into a long, ~11 cm, quartz holder. At the beginning of each experiment, the two holders were placed in an autoclave and 14 ml of NaCl-bearing solution was added to it. This solution covered the short holder but not the long holder, the top of which was predicted to be above the level of the liq-

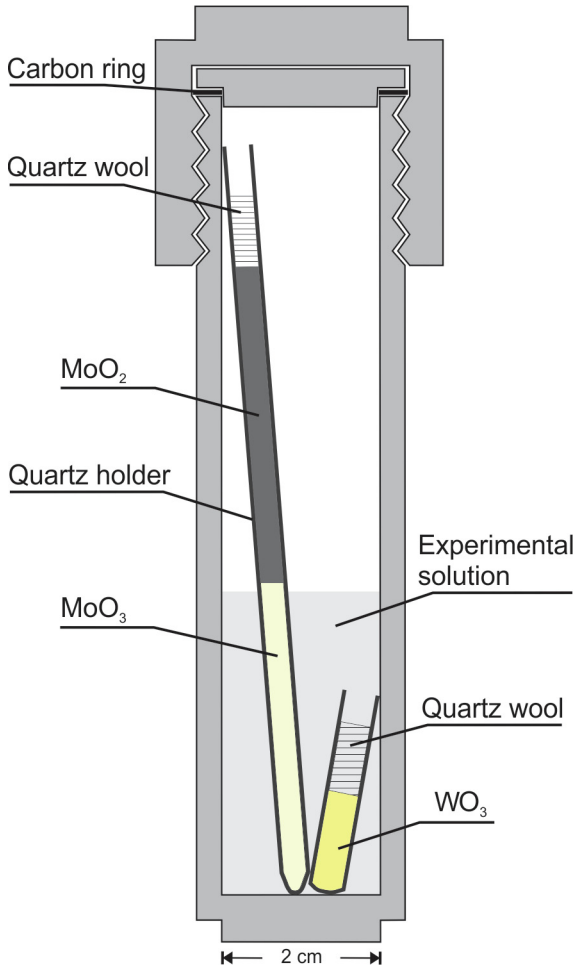

Fig. 1. A schematic diagram showing the experimental set-up employed in this study. Malleable carbon rings provided an airtight seal upon closure of the autoclave.

uid during the experiments (Fig. 1). Prior to sealing, the autoclaves were purged with nitrogen gas to remove atmospheric oxygen.

Kinetic experiments were performed at 250 °C with a 1 mol/L NaCl solution containing 0.01 mol/L HCl for durations between 1 and 11 days. The tungsten concentration reached a steady state value after 6 days (Fig. 2). As experiments conducted at higher temperature were predicted to reach steady state concentrations more rapidly, all subsequent experiments were conducted for durations of $\geq$7 days. At the end of each set of experiments, the autoclaves were removed from the oven and quenched to ambient temperature in less than 20 minutes. A 4 ml aliquot of solution was taken from each autoclave for the determination of pH and analysis of chloride concentration. Four ml of 0.5 wt.% optima grade ammonium hydroxide was then added to each autoclave to dissolve any tungsten that had precipitated on the walls during quenching. After an hour, the mixed solution was removed for analysis of its tungsten content. The pH was measured using an accuTupH™ Rugged Bulb Combination pH Electrode purchased from Fisher Scientific. Solutions containing greater than

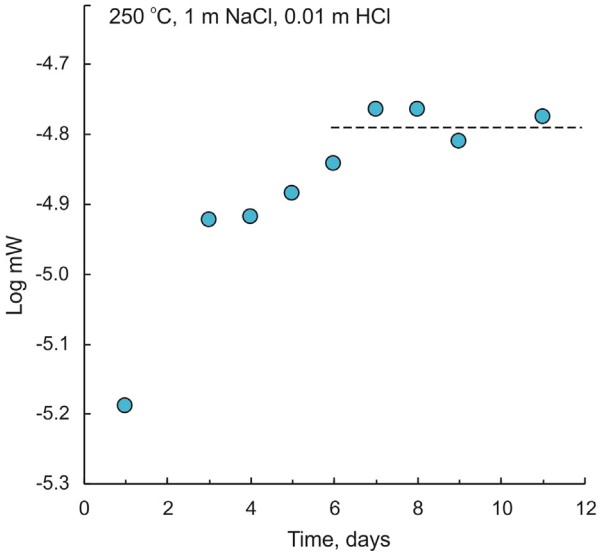

Fig. 2. A diagram showing the results of experiments of variable duration conducted at 250 °C (kinetic experiments) with an aqueous solution containing 1 mol/kg NaCl and 0.01 mol/kg HCl. From the diagram, it is evident that the solubility of $WO_3^{crystal}$ reached a steady state concentration after six days.

0.1 mol/L Na^+ were diluted to a concentration less than this prior to measuring their pH. The resulting pH values were corrected to the corresponding pH values for the temperatures of the experiments using HCh software (Shvarov, 2008). Tungsten concentrations were analyzed using Inductively Coupled Plasma Mass Spectrometry after 1250 to 2500 times dilution of the experimental solution using a 0.001 wt.% optima grade ammonium hydroxide solution. Finally, the WO_3 reactant was analyzed by X-ray diffraction to confirm that new solids had not formed during the experiments and that the measured solubility corresponded only to the dissolution of WO_3; the only phase detected was crystalline WO_3 (Appendix). X-ray diffraction analysis also confirmed that the buffer solids MoO_2 and Mo_2O_3 solid were both present after the experiments.

2.2. Data optimization

The dissolved tungsten species in the solution were identified from the slope of the logarithm of the molality and activity of tungsten with respect to that of the other ions in each experiment. Thermodynamic properties for these species, including the standard Gibbs free energy and formation constants, were determined from the molality of tungsten, NaCl and HCl in each experiment using the program OptimA (masses corresponding to an excess of the solute, WO_3^{cryst}, and the oxygen buffer assemblage at the end of each experiment were also specified in the input file), which is part of the HCh software package (Shvarov, 2015). The activity coefficient of each ionic species was calculated using the extended Debye-Hückel equation (Helgeson et al., 1981; Oelkers and Helgeson, 1990; Oelkers and Helgeson, 1991):

$$\log \gamma_n = -\frac{A \cdot [z_n]^2 \cdot \sqrt{I}}{1 + B \cdot \mathring{a} \cdot \sqrt{I}} + b_\gamma \cdot I + \Gamma \quad (1)$$

in which A and B are constants representing Debye-Hückel limiting law parameters (Table 1), b_γ is the extended parameter for NaCl from Helgeson and Kirkham (1974), $\mathring{a}$ is the distance of closest approach, which is specific to the ion of interest, z is the charge of the ion, Γ is a molarity to molality conversion factor, and I is the ionic strength calculated using Eq. (2):

$$I = \frac{1}{2}\sum_{i=1}^{n} c_i z_i^2 \quad (2)$$

where c_i is the molar concentration of ion i (mol/L) and z_i is the charge of that ion. Parameter I represents the true ionic strength as all the dissolved components were considered. The activity coefficients of neutral species were assumed to be unity. The Haar-Gallagher-Kell and Marshall and Franck models were used to determine the thermodynamic properties and disassociation constant of H_2O for our experimental conditions (Marshall and Franck, 1981; Kestin et al., 1984).

3. RESULTS

3.1. Identification of the dissolved tungsten species

The results of the experiments at 250, 300, and 350 °C are reported in Table 2. In order to determine whether or not tungsten solubility depends on Na^+ (or Cl^-) concentration, sets of experiments were conducted with solutions having roughly constant pH (~2) at ambient temperature and variable NaCl concentration. The pH dependency was evaluated with sets of experiments, each of which was conducted with solutions having approximately the same NaCl concentration (the concentrations of the different sets varied from high to low).

From Fig. 3a, c and e, it is evident that the concentration of tungsten was low and roughly constant at low $a\mathrm{Na}^+$, whereas at higher $a\mathrm{Na}^+$ (the Cl^- activity is very similar to that of Na^+) it increased linearly with log $a\mathrm{Na}^+$. At first glance, these observations suggest that the tungsten species at low Na^+ (or Cl^-) activity was $H_2WO_4^0$ or HWO_4^- or WO_4^{2-}, which do not contain Na or Cl, and that at higher Na^+ (or Cl^-) activity it was a Na-tungstate ion pair or a tungsten-chloride complex. At low $a\mathrm{Na}^+$, the tungsten concentration was independent of pH (Fig. 3(b, d, and f)), which indicates that tungsten solubility was dominated by the neutral tungstate, tungstic acid ($H_2WO_4^0$). In contrast, at high Na^+ (or Cl^-) concentration, the tungsten concentration increased linearly with pH (the slope varied between 0.77 and 0.95). As previous experiments have shown convincingly that Cl^- complexes do not play a role in tungsten dissolution (Wood and Vlassopoulous, 1989; Wood, 1992), the positive correlation of tungsten solubility with pH at high NaCl concentration and also with log $a\mathrm{Na}^+$, could reflect a major contribution from $NaHWO_4^0$ via the reaction:

$$WO_3^{cryst} + H_2O + Na^+ = NaHWO_4{}^0 + H^+ \quad (3)$$

$$\mathrm{Log}\ K_3 = \log a\mathrm{NaHWO_4}{}^0 - \mathrm{pH} - \log a\mathrm{Na}^+$$

An alternative explanation for these correlations is that the increase in WO_3 solubility with increasing log $a\mathrm{Na}^+$ was due to the increase in the ionic strength of the solution that accompanied the addition of NaCl. In order to test this latter hypothesis, we calculated the total activity of tungsten, assuming that the only tungsten species in solution were HWO_4^- and $H_2WO_4^0$. In addition, we normalized all the data for the three experimental temperatures to a pH of 1.8 (350 °C) and 1.4 (300 °C and 250 °C), which are the lowest pH values of the experiments at the three temperatures. The normalization was based on the following reactions and equations:

$$WO_3^{cryst} + H_2O = HWO_4{}^- + H^+ \quad (4)$$

$$\mathrm{Log}\ K_4 = \log a\mathrm{HWO_4}{}^- - \mathrm{pH}$$

$$WO_3^{cryst} + H_2O = H_2WO_4{}^0 \quad (5)$$

$$\mathrm{Log}\ K_5 = \log a\mathrm{HWO_4^0}$$

$$\mathrm{Log}\ a\sum \mathrm{W}\ (\mathrm{adjusted}) = \log(10^{\log\ aHWO_4^- - (pH - pH_{Minimun})} + aH_2WO_4^0) \quad (6)$$

In Fig. 4, we show these normalized data as a plot of $\log a\sum W$ versus pH. From this diagram, it is clear that the logarithm of the adjusted $a\sum W$ is independent of pH. The presence of any $NaHWO_4^0$, in addition to the assumed HWO_4^- and $H_2WO_4^0$, would result in a slope greater than 0 in Fig. 4 as Reaction (3) is not only pH-dependent but also Na-dependent. The absence of such a slope indicates that $NaHWO_4^0$ did not contribute significantly to the total dissolved concentration of tungsten in the experimental solutions.

As discussed above, $NaHWO_4^0$ is interpreted not to have been present in the experimental solutions in detectable concentrations, despite the fact that the solubility of $WO_3^{crystal}$ increased with increasing NaCl concentration.

Table 1
Values for thermodynamic parameters from Helgeson and Kirkham (1974) used in the activity coefficient function (Eq. (1)).

	A		B		$b_{\gamma,\ NaCl}$	
T (°C)	Sat.	1000 bar	Sat.	1000 bar	Sat.	1000 bar
200	0.7994	0.7195	0.3639	0.3591	0.0485	0.0647
250	0.9593	0.8221	0.3766	0.3690	0.0203	0.0485
300	1.2175	0.9502	0.3925	0.3792	−0.0244	0.0278
350	1.8234	1.1178	0.418	0.3902	−0.1076	0.0024
400		1.3502		0.4024		−0.0292

Table 2
Compositions of quenched experimental solutions from experiments. The values of $a\mathrm{Na}^+$ (T) and pH (T) are calculated at interested temperatures.

T (°C)	NaCl(m)	HCl(m), 10^{-3}	W(m), 10^{-6}	pH(25 °C)	$a\mathrm{Na}^+$ (T)	pH (T)
350	1.40	5.59	611	2.48	0.10	3.65
350	1.40	6.49	452	2.42	0.10	3.60
350	1.40	11.4	337	2.17	0.10	3.37
350	1.40	19.2	201	1.95	0.10	3.15
350	1.40	30.8	180	1.74	0.10	2.95
350	1.40	50.7	96.0	1.52	0.10	2.73
350	1.25	6.68	432	2.40	0.10	3.56
350	1.00	6.63	349	2.39	0.09	3.52
350	0.85	8.51	230	2.28	0.08	3.39
350	0.70	7.65	270	2.32	0.07	3.39
350	0.70	10.7	218	2.17	0.07	3.25
350	0.70	19.8	137	1.91	0.07	2.99
350	0.70	27.8	84.2	1.76	0.07	2.84
350	0.70	42.3	69.9	1.58	0.07	2.66
350	0.70	70.5	55.0	1.36	0.07	2.44
350	0.40	9.35	106	2.21	0.05	3.19
350	0.40	10.9	143	2.14	0.05	3.12
350	0.40	9.27	152	2.21	0.05	3.19
350	0.30	13.7	78.6	2.03	0.05	2.96
350	0.30	8.65	94.9	2.23	0.05	3.16
350	0.20	13.2	67.6	2.03	0.04	2.89
350	0.10	11.5	72.6	2.06	0.02	2.81
350	0.10	11.2	62.6	2.07	0.02	2.82
350	0.085	11.9	37.7	2.04	0.02	2.77
350	0.07	10.6	28.9	2.08	0.02	2.78
350	0.05	8.21	41.0	2.18	0.02	2.82
350	0.02	8.06	25.8	2.17	0.01	2.67
350	0.01	6.30	33.6	2.26	0.005	2.67
350	0.01	11.4	40.0	2.01	0.005	2.45
350	0.01	16.0	39.2	1.87	0.004	2.33
350	0.01	28.5	33.1	1.63	0.004	2.14
350	0.01	32.6	30.6	1.57	0.004	2.10
350	0.01	42.5	30.1	1.46	0.004	2.02
350	0.01	56.7	32.6	1.35	0.003	1.94
350	0.01	71.3	34.3	1.26	0.003	1.87
350	0.0005	11.5	27.5	1.99	0.0003	2.32
350	0.0005	9.20	27.5	2.08	0.0003	2.39
300	3.00	5.07	188	2.55	0.37	3.31
300	3.00	5.15	174	2.55	0.37	3.30
300	3.00	5.13	148	2.55	0.37	3.31
300	2.00	6.53	81.3	2.43	0.30	3.12
300	2.00	7.49	79.3	2.37	0.30	3.06
300	2.00	6.82	87.4	2.41	0.30	3.10
300	1.40	1.82	396	2.97	0.24	3.55
300	1.40	2.77	251	2.79	0.24	3.40
300	1.40	4.22	162	2.60	0.24	3.23
300	1.40	7.63	119	2.35	0.24	2.98
300	1.40	13.6	46.4	2.11	0.24	2.74
300	1.40	21.7	46.6	1.89	0.24	2.53
300	1.40	24.1	29.3	1.85	0.24	2.49
300	1.00	9.76	52.1	2.23	0.20	2.81
300	0.90	10.5	64.9	2.19	0.19	2.76
300	0.80	10.9	44.1	2.02	0.17	2.72
300	0.70	9.73	47.2	2.21	0.16	2.74
300	0.70	11.5	39.7	2.14	0.16	2.67
300	0.70	9.05	59.5	2.25	0.16	2.78
300	0.40	9.39	37.8	2.21	0.11	2.66
300	0.30	10.4	25.7	2.15	0.09	2.56
300	0.25	10.3	22.1	2.15	0.08	2.54

(*continued on next page*)

Table 2 (*continued*)

T (°C)	NaCl(m)	HCl(m), 10^{-3}	W(m), 10^{-6}	pH(25 °C)	$a\mathrm{Na}^+$ (T)	pH (T)
300	0.20	9.62	28.7	2.17	0.07	2.53
300	0.10	8.29	16.3	2.20	0.04	2.49
300	0.085	10.6	19.1	2.09	0.04	2.37
300	0.07	10.4	16.7	2.14	0.03	2.35
300	0.04	9.48	23.9	2.11	0.02	2.32
300	0.01	1.79	24.3	2.80	0.01	2.90
300	0.01	16.6	14.5	1.85	0.01	2.01
300	0.01	17.8	9.84	1.82	0.01	1.98
300	0.01	25.4	13.0	1.67	0.01	1.85
300	0.01	27.2	17.7	1.65	0.01	1.83
300	0.01	28.1	7.34	1.63	0.01	1.82
300	0.01	37.3	16.7	1.52	0.01	1.72
300	0.01	43.6	7.10	1.45	0.01	1.67
300	0.01	58.4	20.6	1.34	0.01	1.57
300	0.01	71.0	22.4	1.26	0.005	1.51
300	0.01	75.1	10.1	1.23	0.005	1.49
300	0.01	75.5	17.5	1.23	0.005	1.49
300	0.01	78.0	9.16	1.22	0.005	1.48
300	0.01	101	21.7	1.12	0.005	1.40
300	0.005	11.5	12.1	2.00	0.003	2.12
300	0.005	9.77	10.4	2.06	0.004	2.18
250	4.00	2.56	67.8	2.86	0.74	3.31
250	4.00	2.96	67.8	2.80	0.74	3.25
250	3.00	5.00	40.4	2.56	0.62	2.98
250	2.00	7.27	23.2	2.38	0.48	2.75
250	1.40	5.53	31.3	2.49	0.38	2.82
250	1.40	8.65	18.1	2.29	0.38	2.63
250	1.40	14.1	14.0	2.08	0.38	2.42
250	1.40	19.7	10.2	1.93	0.38	2.27
250	1.40	31.7	5.92	1.73	0.38	2.07
250	1.00	9.78	11.6	2.23	0.30	2.53
250	0.70	11.5	11.1	2.14	0.24	2.41
250	0.40	12.3	8.31	2.09	0.16	2.31
250	0.30	12.8	12.1	2.06	0.13	2.26
250	0.25	11.3	11.5	2.11	0.11	2.29
250	0.20	12.8	10.1	2.04	0.09	2.22
250	0.01	24.7	5.44	1.69	0.007	1.77
250	0.01	28.1	3.02	1.63	0.007	1.72
250	0.01	37.5	6.92	1.51	0.007	1.61
250	0.01	38.0	8.92	1.51	0.007	1.60
250	0.01	44.8	6.51	1.44	0.006	1.54
250	0.01	59.5	6.97	1.33	0.006	1.44
250	0.01	60.3	4.99	1.32	0.006	1.44
250	0.01	60.5	8.06	1.32	0.006	1.43
250	0.01	73.6	10.1	1.24	0.006	1.36
250	0.01	74.8	3.83	1.24	0.006	1.36
250	0.0005	2.75	12.5	2.59	0.0004	2.61
250	0.0005	1.77	17.5	2.77	0.0005	2.79
250	0.0005	7.63	6.52	2.16	0.0004	2.20

Instead, we conclude that the solubility data can be satisfactorily explained by HWO_4^- and $H_2WO_4^0$. From Fig. 5, it can be seen that the tungsten activity was low and constant at low pH and at higher pH increased with increasing pH at each of the temperatures for which the solubility of $WO_3^{crystal}$ was determined. The independence of tungsten activity from pH at low values of pH was due to the formation of $H_2WO_4^0$ according to Reaction (5), which does not involve H^+. At higher pH values, the increase in tungsten activity with increasing pH was due to the formation of HWO_4^- via Reaction (4), inspection of which reveals that $a\mathrm{HWO}_4^-$ increases with decreasing $a\mathrm{H}^+$ or increasing pH in a ratio of 1:1. This interpretation is supported by the observation that the slope of the dependency of log $a\mathrm{HWO}_4^-$ on pH ranges between 0.93 and 1.17, depending on the temperature (Fig. 5(b, d and f)). The threshold pH above which HWO_4^- replaces $H_2WO_4^0$ as the dominant species is 2.44 at 350 °C (Fig. 5a) and corresponds to a tungsten concentration of ~5.9 ppm. This threshold pH at 300 °C is 2.32, corresponding to a tungsten concentration of ~2.7 ppm and at 250 °C is 2.22, corresponding to a tungsten concentration of ~1.2 ppm.

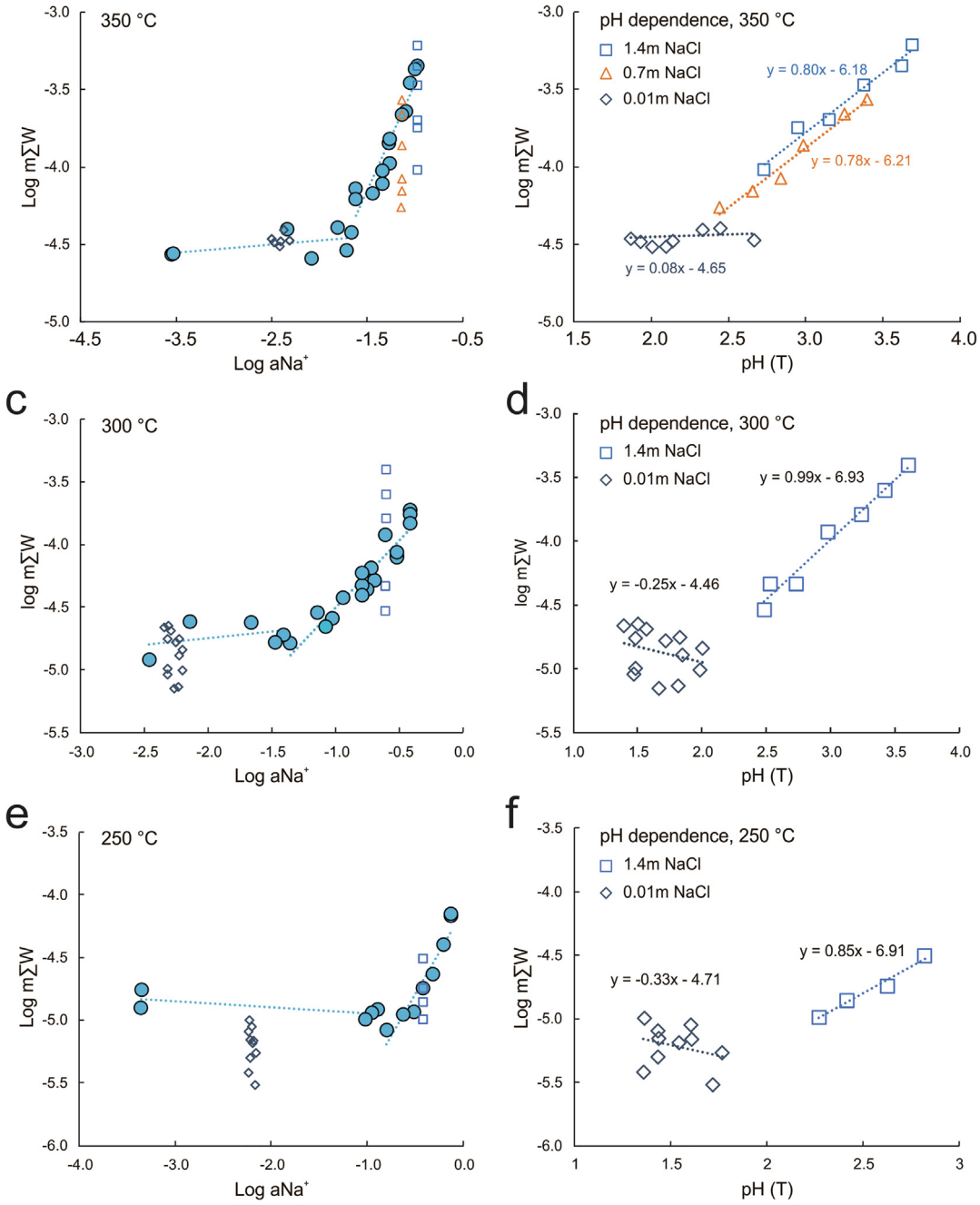

Fig. 3. Results of experiments at 350 °C, 300 °C, 250 °C. (a), (c), and (e) showing the concentrations of dissolved tungsten (log mΣW) as a function of the activity of Na^+ (log aNa^+) and (b)–(f) the tungsten concentrations as a function of pH. The filled blue circles in (a), (c), (e) represent the results of experiments designed to determine the dependence of the solubility of WO_3 on Na^+ activity at a $pH_{(25\ °C)}$ of ~2. The results of experiments designed to determine the dependence of WO_3 solubility on pH (at nearly constant log aNa^+) are illustrated in (d)–(f); the data for these experiments are also shown in (a), (c), (e) using the symbols employed in (d)–(f). The equations "y = ax - b" represent linear regressions of the data. (For interpretation of the references to colour in this figure legend, the reader is referred to the web version of this article.)

3.2. Evaluation of formation constants (β)

As mentioned above, the standard Gibbs free energy for $H_2WO_4^0$ and HWO_4^- were determined from the molality of NaCl, HCl, and tungsten in each experiment using the program OptimA in the HCh software package (Shvarov, 2015); the molality of HCl was calculated from the starting NaCl concentration and the pH measured after each experiment. In addition to the two tungsten species, the following aqueous species were also considered in the calculations:

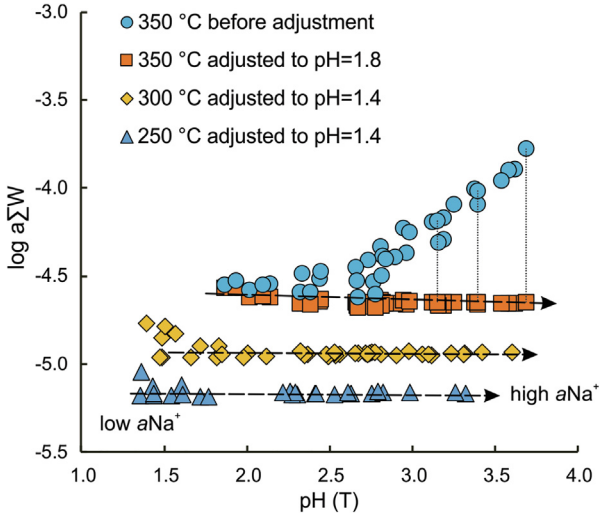

Fig. 4. A plot showing values of log $a\sum$W at 350, 300, 250 °C as a function of pH, assuming that the solubility of $WO_3^{crystal}$ can be fully explained by its dissolution as $H_2WO_4^0$ and HWO_4^-. The log $a\sum$W values were adjusted to pH (T) = 1.8 (350 °C), and pH (T) = 1.4 (300 and 250 °C) on the basis of the stoichiometry of Reactions (4) and (5). The log $a\sum$W values at 350 °C prior to the adjustment are shown for comparison. The dashed lines with arrowheads indicate the trends of tungsten activity from low to high sodium ion activity.

O_2, H_2, H^+, OH^-, Na^+, Cl^-, $NaOH^0$, $NaCl^0$, and HCl^0. Thermodynamic data for these species were obtained from Johnson et al. (1992), Shock et al. (1997), and Sverjensky et al. (1997) and values for the extended parameter for NaCl were taken from Oelkers and Helgeson (1991). Thermodynamic data for the tungsten and molybdenum oxide solids (WO_3, MoO_2 and MoO_3) were taken from Pankratz and Mrazek (1982) and Robie and Hemingway (1995). The sources of these data are listed in the Appendix.

With the standard Gibbs free energy of HWO_4^- and $H_2WO_4^0$ in hand, the Gibbs free energy changes for the reactions responsible for the formation of these species were calculated using the standard Gibbs free energy of the other species involved in the reactions, namely WO_4^{2-} and H^+.

$$H^+ + WO_4{}^{2-} = HWO_4{}^- \quad (7)$$

$$2H^+ + WO_4{}^{2-} = H_2WO_4{}^0 \quad (8)$$

Thermodynamic data for WO_4^{2-} and H^+ were taken from Shock et al. (1997) and Wesolowski et al. (1984). The Gibbs free energy change was then converted to a formation constant (log β) using the relationship $\Delta G^\circ = -RT\ln K$. These formation constants and the uncertainty associated with their determination are listed in Table 3; the uncertainty was calculated using the OptimA program. The formation constants for $H_2WO_4^0$ and HWO_4^- at the different temperatures were fitted to the Bryzgalin-Ryzhenko model (Ryzhenko et al., 1985) modified by Shvarov and Bastrakov (1999):

$$\log K_{(T,P)} = \frac{T_r}{T}\log K_{(T_r,P_r)} + B_{(T,P)}\left(A_{zz/a} + \frac{B_{zz/a}}{T}\right) \quad (9)$$

values for the parameters of which are listed in Table 4. In the equation, K is the dissociation constant of the ion pair, T_r, P_r are the reference temperature and pressure, and $A_{zz/a}$ and $B_{zz/a}$ are fitting parameters. The term $B_{(T,P)}$ was computed from the dissociation constant of water (Marshall and Franck, 1981) at temperature T and pressure P. This fit was then used to calculate equilibrium constants (log K) for the tungsten oxide dissolution reactions. These values are reported in Table 5. Uncertainties in the equilibrium constants were determined by calculating the log K values of each data point using the tungsten activity, pH(T), and Reactions (4) and (5), and then calculating the standard deviation of these values, at each temperature. The best fit points to the experimental data shown in Figs. 5–8 were calculated from these equilibrium constants.

4. DISCUSSION

4.1. Comparison to previous studies

Previous estimates of the thermodynamic properties of tungsten species have been based mainly on the potentiometric experiments of Wesolowski et al. (1984) and the solubility experiments of Wood and Vlassopoulos (1989) and Wood (1992). Wesolowski et al. (1984) showed that the tungstates, HWO_4^- and WO_4^{2-}, are the dominant tungsten species in mildly to strongly saline aqueous solutions at temperatures between 150 and 300 °C and near-neutral to alkaline conditions, respectively, and that tungstic acid is the dominant species at low pH. Shock et al. (1997) developed a HKF model for WO_4^{2-} and HWO_4^- based on the results of the experiments of Wesolowski et al. (1984), which are widely used in evaluating tungsten solubility in hydrothermal fluids (Heinrich, 1990; Gibert et al., 1992; Wood and Samson, 2000).

Wood and Vlassopoulos (1989) concluded that the ion pair, $NaHWO_4^0$, is the dominant aqueous species in solutions with high salinity based on experimental determinations of the solubility of $WO_3^{crystal}$ in solutions containing up to 6 m NaCl and 1 m NaOH at 500 °C and 1 kbar. However, although they concluded that $H_2WO_4^0$ is the dominant species at low pH, they did not consider HWO_4^- in their calculation of the speciation of tungsten at higher pH and NaCl concentration. They also assumed that the activity coefficients of the tungsten species were equal to unity. In order to determine whether the results of their experiments could be explained without calling upon a sodium tungstate species, we calculated the dissolved tungsten concentration at the conditions of their experiments using the thermodynamic data from this study and that of Wood and Vlassopoulos (1989), assuming that tungsten was present in their solutions only as the species $H_2WO_4^0$ and HWO_4^- (this study) and WO_4^{2-} (Wesolowski et al., 1984). The calculated tungsten concentration is very similar to that measured in the experiments of Wood and Vlassopoulos (1989) involving NaOH and NaCl, even at the highest concentrations of these solutes (Fig. 6(a and b)). This suggests strongly that HWO_4^- or WO_4^{2-} and not $NaHWO_4^0$ were the dominant species in these experiments at mildly acidic and alkaline pH, respectively. The addition of NaCl or NaOH

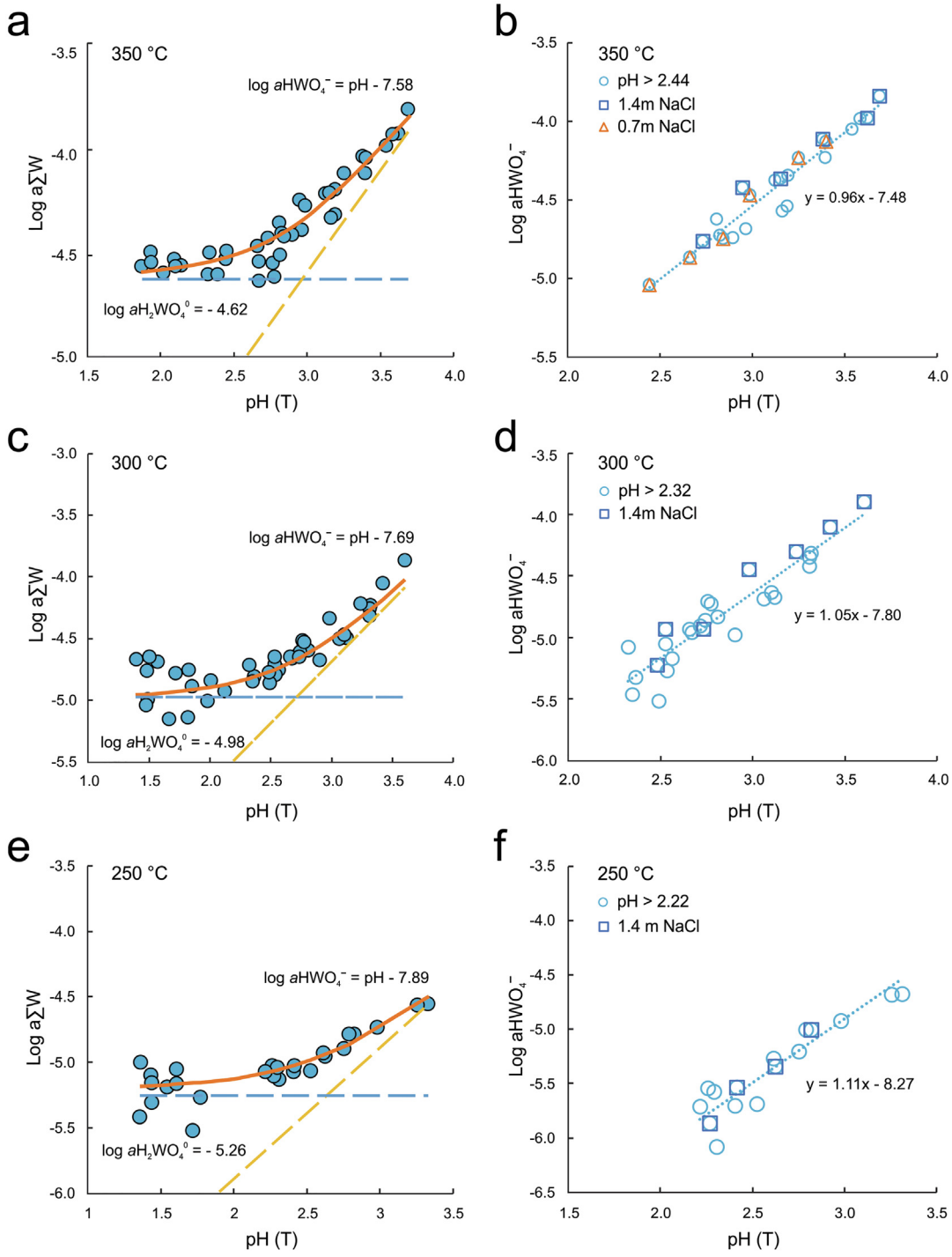

Fig. 5. Plots of log $a\sum W$ and log $a HWO_4^-$ versus pH (T) at 350 °C (a, b), 300 °C (c, d), and 250 °C (e, f). The filled blue circles in (a), (c), (e) represent the results of the experiments at the temperature of interest, the orange curves show the fits to the data based on the log K values for Reactions (4) and (5) and the yellow and blue dashed lines indicate the activity of HWO_4^- and $H_2WO_4^0$ based on the log K values for Reaction (4) and (5), respectively. The parameters $a\sum W$, $aHWO_4^-$, and pH (T) refer to the total tungsten activity, the activity of HWO_4^-, and the pH of the experimental solution at each temperature, respectively. The dotted lines represent the best fits to the data for $aHWO_4^-$ versus pH (T) at the different temperatures and "y = ax − b" the equations of these lines. Diagrams (a), (c) and (e) illustrate the independence of tungsten activity from pH at low pH values due to the dissolution of $WO_3^{crystal}$ as $H_2WO_4^0$, and its dependence on pH at high pH values because of the formation of HWO_4^-.

Table 3
Formation constants (log β) for the tungsten species identified in this study based on experiments between 250 and 350 °C.

	250 °C	300 °C	350 °C
$WO_4^{2-} + 2H^+ = H_2WO_4^0$	8.23 ± 0.01	9.20 ± 0.01	10.96 ± 0.01
$WO_4^{2-} + H^+ = HWO_4^-$	5.58 ± 0.02	6.51 ± 0.01	7.99 ± 0.01

Table 4
Bryzgalin-Ryzhenko parameters derived for tungsten species based on the formation constants determined in this study.

	pK (298)	A (zz/a)	B (zz/a)
$H_2WO_4^0$	6.570	1.412	0.000
HWO_4^-	3.413	1.150	0.000

to the solutions increases the ionic strength as well as pH and, in turn, decreases the activity coefficient and increases the concentration of HWO_4^-, respectively. We note, however, that the tungsten concentrations in our acidic, lower pH experiments are lower than those of Wood and Vlassopoulos (1989). We attribute this discrepancy as probably being due to entrainment of solute particles during sampling in the experiments of Wood and Vlassopoulos (1989). The line fit to their data by Gibert et al. (1992), suggesting higher tungsten concentrations than predicted by our data, results from the higher logK_5 values proposed for Reaction (5).

As has already been mentioned, Wood (1992) determined the solubility of $WO_3^{crystal}$ in aqueous solutions with variable HCl concentrations at temperatures between 300 and 600 °C and 1 kbar. He demonstrated that $H_2WO_4^0$ is the principal tungsten species at all HCl concentrations and calculated log K values for the dissolution reaction (Reaction (5), this study). We extrapolated our data and those of Wood (1992) using the Bryzgalin-Ryzhenko model at saturated water vapor pressure and 1kbar, respectively, in order to compare the two data sets. His log K values for this reaction are 1–2 units higher than the values determined in this study (Table 6). A possible reason for this discrepancy is that he did not consider the possible formation of HWO_4^- at low HCl concentration. We cannot explain, however, why the log K values reported by Wood (1992) are systematically higher than those reported in this study.

Wood and Samson (2000) proposed that, in natural systems, tungsten is transported as the species $H_2WO_4^0$, HWO_4^-, WO_4^{2-}, $NaHWO_4^0$, and $NaWO_4^-$. They calculated formation constants for $H_2WO_4^0$ HWO_4^-, and WO_4^{2-} based on the results of the experiments of Wood (1992) and Wesolowski et al. (1984). However, in the absence of the necessary data for $NaHWO_4^0$ and $NaWO_4^-$, they assumed that the formation constants for these species are equal to those for $KHSO_4^0$ and KSO_4^-. In order to determine whether the thermodynamic data recommended by Wood

Table 5
Logarithms of equilibrium constants (logK) and their associated uncertainty for the WO_3 dissolution reactions.

	250 °C	300 °C	350 °C
$WO_3^{cryst} + H_2O = H_2WO_4^0$	−5.26 ± 0.26	−4.98 ± 0.25	−4.62 ± 0.10
$WO_3^{cryst} + H_2O = HWO_4^- + H^+$	−7.89 ± 0.30	−7.69 ± 0.29	−7.58 ± 0.18

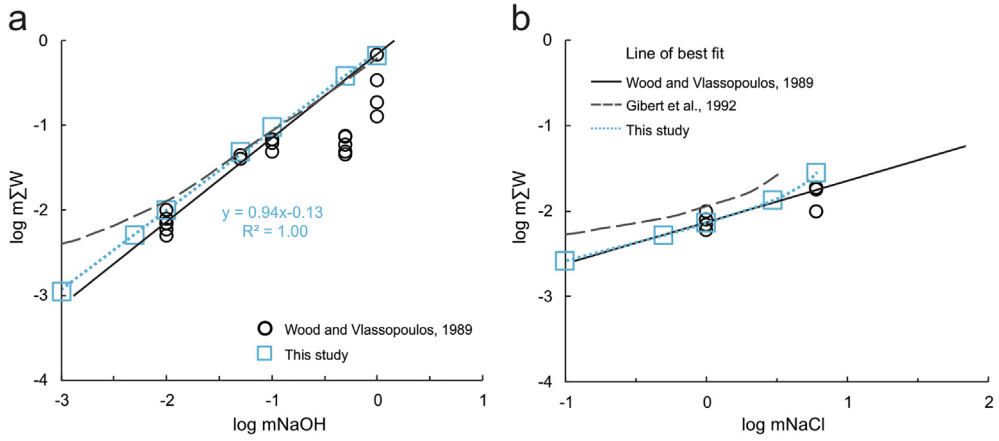

Fig. 6. (a) A comparison of the fit to the data for log mΣW as a function of log mNaOH reported in this study to those for the data of Wood and Vlassopoulos (1989 500 °C and 1000 bar) and those of Wood and Vlassopoulos (1989) recalculated by Gibert et al. (1992). (b) A comparison of the fit to the data for log mΣW as a function of log mNaCl reported in this study to those for the data of Wood and Vlassopoulos (1989) and those of Wood and Vlassopoulos (1989) recalculated by Gibert et al. (1992). The tungsten species used in the calculation were $H_2WO_4^0$, HWO_4^-, and WO_4^{2-}. See text for further detail.

and Samson (2000) are consistent with our experimental data, we calculated the concentration of tungsten that we expected to observe in each of our experiments, based on their data. In Fig. 7, we compare the results of our experiments with these predictions in plots of log m∑W versus log $a\mathrm{Na}^+$ and pH (T) for 250, 300 and 350 °C. As is evident from this figure, the concentration of tungsten observed in our experiments is 1–2 log units lower than that predicted from the thermodynamic data of Wood and Samson (2000) at equivalent conditions.

For an additional comparison, we made use of the association constant reported earlier for HWO_4^- (Reaction (7)) and the association constant for $H_2WO_4^0$ calculated using the thermodynamic data from for the following reaction:

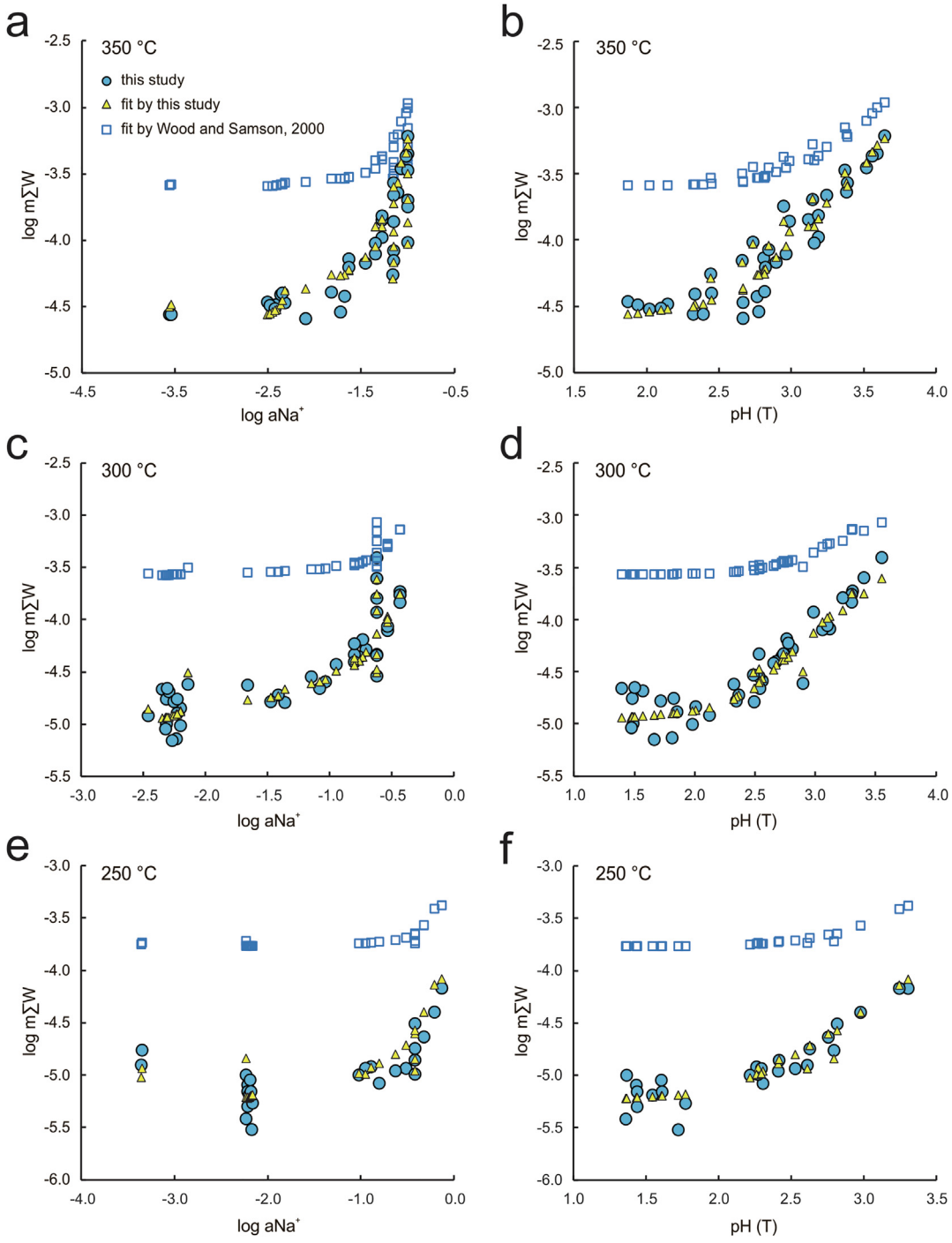

Fig. 7. Plots of log $a\sum W$ versus log $a\mathrm{Na}^+$ and log $a\sum W$ versus pH comparing the results of the experiments conducted in this study with the expected log $a\sum W$ values of these experiments calculated using log K values reported by Wood and Samson (2000) based on the results of the experiments of Wood (1992) for 350 °C (a), 300 °C (c), 250 °C (e, f) and water saturated vapor pressure.

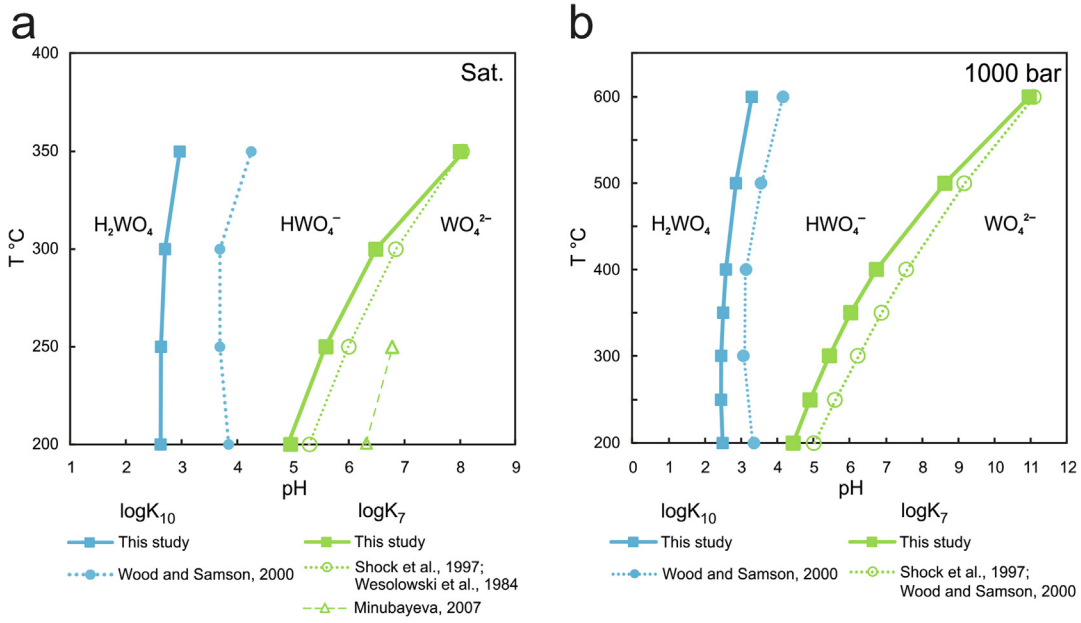

Fig. 8. Predominance fields for $H_2WO_4^0$, HWO_4^-, and WO_4^{2-} in aqueous liquid as a function of temperature and pH at saturated vapor pressure (a) and 1000 bar (b) based on the results of this study; thermodynamic data for WO_4^{2-} were taken from Shock (1992). Also shown are the predominance fields for these species based on the experimental data of Wesolowski et al. (1984), Wood and Samson (2000), and Minubaeva (2007).

$$HWO_4^- + H^+ = H_2WO_4^0 \quad (10)$$

$$\log K_{10} = \log a H_2WO_4^0 - \log a HWO_4^- + pH$$

In Table 6, we compare the association constants for Reactions (7) and (10) calculated in this study with those of previous studies. Our values are considerably lower than those reported previously, largely because the latter were based on the data of Wood (1992), which we believe overestimated the solubility of tungsten. We use these association constants in Fig. 8 to predict the predominance fields of $H_2WO_4^0$, HWO_4^- and WO_4^{2-}. Our constants predict that $H_2WO_4^0$ is dominant only at pH values <2.8, which is over one unit less than that predicted previously. The disparity is somewhat less for the dominance of WO_4^{2-}, with our values predicting a predominance boundary at a pH of 5 for 200 °C and vapor-saturated water pressure, which is only 0.3 units less than that predicted by other studies except that of Minubaeva (2007), whose data are not consistent with those of other studies.

4.2. Application to natural systems

Tungsten is deposited as the minerals scheelite ($CaWO_4$) and wolframite ((Fe, Mn)WO_4) in ore-forming hydrothermal systems. Here we make use of the results of our experimental study to quantitatively evaluate the conditions under which tungsten transport is optimized and those that promote the deposition of scheelite and wolframite. For simplicity, we represent wolframite by its endmember, ferberite ($FeWO_4$). Thermodynamic data for the minerals were taken from Holland and Powell (1998), Wood and Samson (2000) and Robie and Hemingway (1995), and for aqueous species other than the tungsten species from Johnson et al. (1992), Shock et al. (1997), Sverjensky et al. (1997) and Tagirov et al. (1997). This information is detailed in in Appendix.

4.2.1. Chloride ion concentration

Although we have shown that ion pairs involving Na^+ and complexes involving Cl^- do not contribute to tungsten solubility in hydrothermal fluids, chloride is important for the transport of both Ca^{2+} and Fe^{2+}, which participate in the formation of scheelite and ferberite, respectively. In fact, Wood and Samson (2000) proposed that high chloride activity in the fluid facilitates the dissolution of tungsten species via the reaction:

$$MWO_4 + mH^+ + nCl^- = H_mWO_4^{(m-2)} + MCl_n^{(2-n)} \quad (11)$$

$$M = Ca^{2+} \text{ or } Fe^{2+}; \quad m = 0 \text{ to } 2; \quad n = 0 \text{ to } 2 \text{ or } 4$$

4.2.2. Temperature

In order to evaluate the effect of cooling on the precipitation of tungsten minerals, we modeled the concentration of tungsten as a function of temperature at conditions of scheelite or ferberite saturation. The results of this modeling show that scheelite and ferberite both precipitate from the solution with decreasing temperature (Fig. 9(a and b)). However, only a small amount of scheelite precipitated from the scheelite-saturated solution, and the tungsten concentration of the solution did not decrease appreciably from its initial concentration. In contrast, almost all the tungsten in the ferberite-saturated solution precipitated (as fer-

Table 6
Association constants and solubility products for tungsten species derived from this and previous studies.

Association constants (log K)

	T (°C)	200	250	300	350	400	500	600	P bars	Method	Reference
$logK_{10}$	$HWO_4^- + H^+ = H_2WO_4^0$	2.63 [d]	2.63	2.71	2.96				Sat.	MBR model	*This study*
		4.20	4.10	3.90	3.90				Sat.	Calculation[a]	Heinrich (1990)
				4.30					Sat.	Calculation[b]	Gibert et al. (1992)
		3.85	3.68	3.70	4.25				Sat.	MBR model extrapolation[c]	Wood and Samson (2000)
		3.56		3.39		3.96			500	HKF model extrapolation[e]	Wood and Samson (2000)
							5.50		1000	Calculation[b]	Gibert et al. (1992)
		3.37		3.08		3.14	3.57	4.16	1000	HKF model extrapolation[e]	Wood and Samson (2000)
		2.52	2.48	2.48	2.51	2.59	2.88	3.31	1000	MBR model extrapolation[d]	*This study*
$logK_7$	$WO_4^{2-} + H^+ = HWO_4^-$	4.96 [d]	5.60	6.47	8.00				Sat.	MBR model	*This study*
		5.34	6.07	6.89					Sat.	Potentiometric measurement	Wesolowski et al. (1984)
		6.31	6.79						Sat.	Uv–vis spectroscopy	Minubaeva (2007)
		5.40	6.10	6.90	7.70				Sat.	Calculation[a]	Heinrich (1990)
				6.90						Calculation[b]	Gibert et al. (1992)
		5.29	6.00	6.85	8.04				Sat.	HKF model extrapolation[e]	Shock et al. (1997)
		5.15		6.48		8.10			500	HKF model extrapolation[e]	Wood and Samson (2000)
							8.10			Calculation[b]	Gibert et al. (1992)
		5.03		6.23		7.58	9.17	11.10	1000	HKF model extrapolation[e]	Wood and Samson (2000)
		5.02	5.61	6.23	6.88	7.58	9.17	11.09	1000	HKF model extrapolation[e]	Shock et al. (1997)
		4.47	4.93	5.44	6.03	6.73	8.63	10.98	1000	MBR model extrapolation[d]	*This study*

Solubility constants (pK = -log K)

	T °C	200	250	300	350	400	500	600	P bars		References
pK_5	$WO_3^{cryst} + H_2O = H_2WO_4^0$		5.26	4.98	4.62				Sat.	Solubility experiment	*This study*
			3.81	3.61	3.29				Sat.	MBR model extrapolation[c]	Wood and Samson (2000)
							2.55		1000	Solubility experiment	Wood and Vlassopoulos (1989)
				4.00		3.40	3.10	2.70	1000	Solubility experiment	Wood (1992)
							2.55		1000	Calculation[b]	Gibert et al. (1992)
		5.77	5.42	5.17	4.97	4.80	4.50	4.60	1000	MBR model extrapolation[d]	*This study*
pK_4	$WO_3^{cryst} + H_2O = HWO_4^- + H^+$		7.89	7.69	7.58				Sat.	Solubility experiment	*This study*
			7.50	7.31	7.54				Sat.	HKF model extrapolation[e]	Shock et al. (1997)
		7.73	7.22	6.86	6.63	6.54	6.83	7.81	1000	HKF model extrapolation[e]	Shock et al. (1997)
		8.29	7.90	7.65	7.49	7.39	7.38	7.92	1000	MBR model extrapolation[d]	*This study*

Note:
[a] Calculated from Wesolowski et al. (1984).
[b] Calculated from Wesolowski et al. (1984) and Wood and Vlassopoulos (1989).
[c] Calculated from MBR (Bryzgalin-Ryzhenko Model) parameters based on the data of Wood and Samson (2000).
[d] Calculated from MBR (Bryzgalin-Ryzhenko Model) parameters based on data from this study.
[e] Calculated from HKF (Helgeson-Kirkham-Flowers Model) parameters.

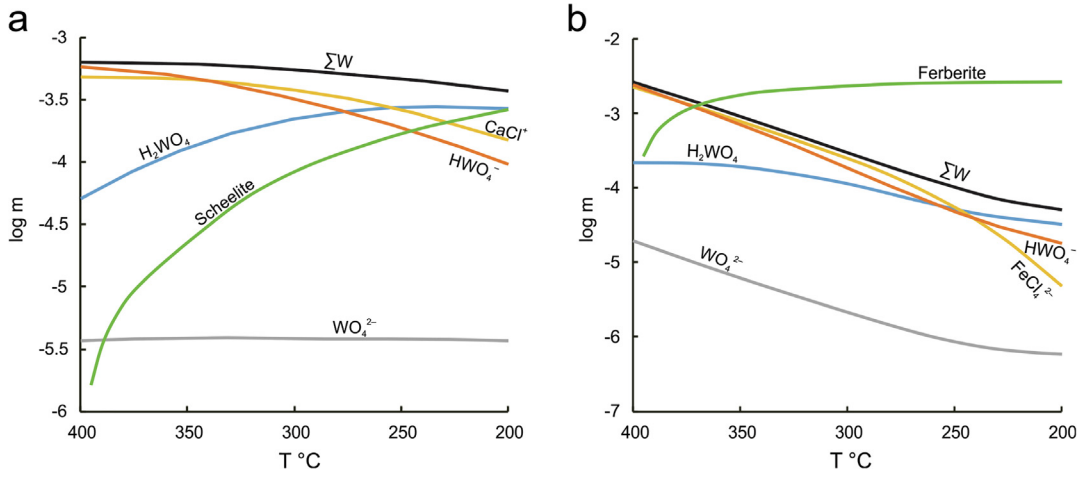

Fig. 9. Plots showing the concentrations of aqueous species and tungsten mineral solubility as a function of temperature. The fluid contained 1.5 m NaCl, 0.02 m HCl, at 400 °C, 1000 bar, and a pH of 3.05 and was saturated with respect to scheelite (a) and ferberite (b).

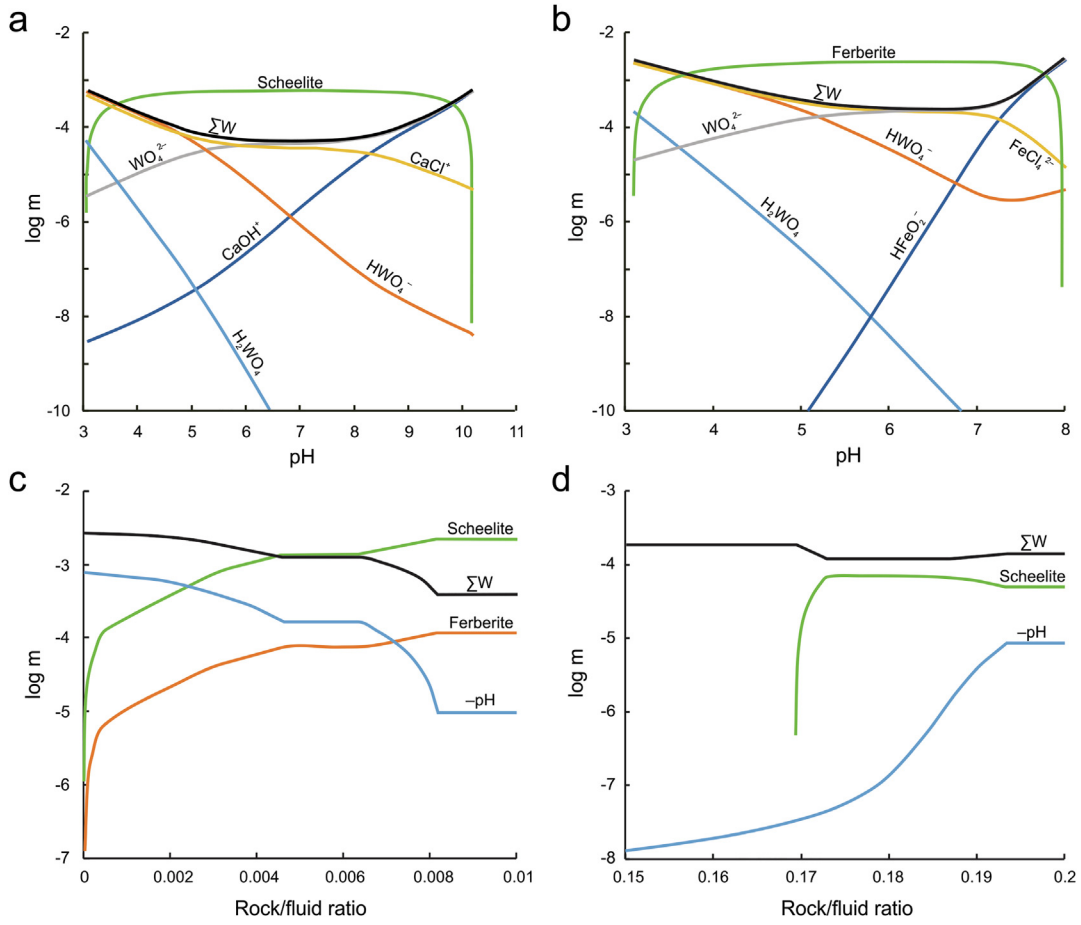

Fig. 10. (a) and (b) Plots showing the concentration of aqueous species and tungsten mineral solubility as a function of increasing pH. The fluid contained 1.5 m NaCl and 0.02 m HCl, at 400 °C, 1000 bar and an initial pH of 3.05, and was saturated with respect to scheelite and ferberite. It was titrated with NaOH to produce the pH increase. (c) A plot showing the total tungsten concentration, pH and tungsten mineral solubility resulting from progressive interaction of the fluid with microcline. The fluid contained 1.5 m NaCl and 0.02 m HCl, at 400 °C, 1000 bar and an initial pH of 3.05, was saturated with respect to scheelite and ferberite, and was buffered to a final pH of ~5. (d). A plot showing the total tungsten concentration, pH and tungsten mineral solubility resulting from progressive interaction of the fluid with a greisen (quartz-muscovite-paragonite). The fluid contained 1.5 m NaCl, 0.1 m NaOH, at 400 °C, 1000 bar and an initial pH of 9.15, was saturated with respect to scheelite and ferberite, and was buffered to a final pH of ~5. The Rock/fluid ratio in (c) and (d) represents the mass of minerals over the mass of fluid.

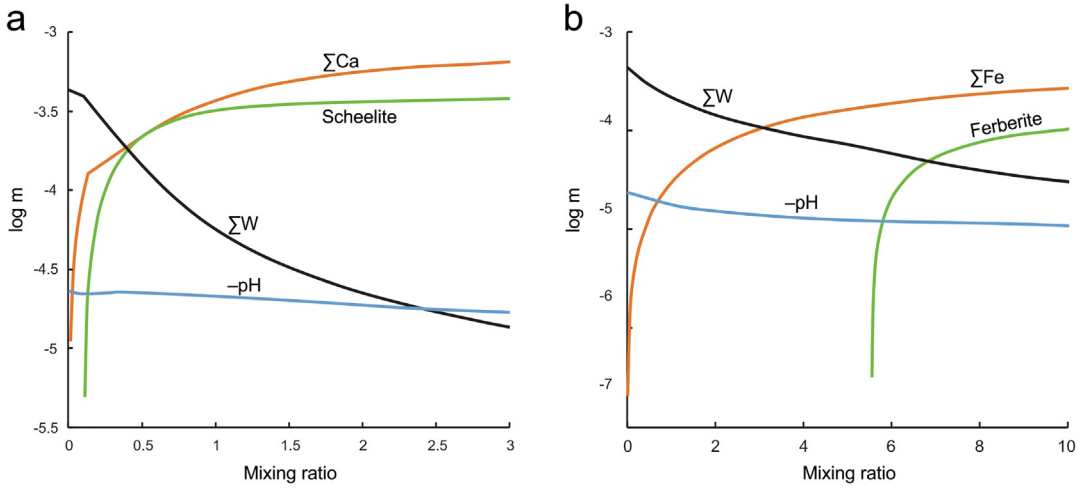

Fig. 11. Plots showing the effect on tungsten concentration and tungsten mineral solubility of mixing an ore fluid containing 4 m NaCl, 0.0003 m HCl and 80 ppm tungsten at 400 °C, 1000 bar, and a pH of 4.64 with a fluid at the same temperature and pressure containing 0.6 m NaCl, 0.0001 m HCl and 0.001 m $CaCl_2$ (a) and 0.6 m NaCl, 0.0001 m HCl and 0.001 m 0.001 m $FeCl_2$ (b). The mixing ratio represents the mass of the second fluid over that of the ore fluid.

berite). This difference in behavior indicates a stronger dependence of the solubility of ferberite on temperature than that of scheelite.

4.2.3. pH

As shown by the results of this experimental study, the solubility of the WO_3 and the nature of the dominant aqueous tungsten species are strongly affected by pH. However, the manner in which pH affects the solubility of the tungsten minerals in natural systems is unclear. We also note that the pH of ore-forming fluid is commonly controlled by fluid-rock interaction. To this end, we modeled the solubility of scheelite and ferberite in a brine as a function of pH (Fig. 10(a and b)), and evaluated the effect of fluid-rock interaction on pH and on the solubility of tungsten in an ore-forming fluid (Fig. 10(c and d)). The results of this modeling show that scheelite and ferberite dissolve in acidic and alkaline solutions, but deposit from solutions with near neutral pH. In the strongly acidic solutions, scheelite and ferberite dissolved via Reaction (11), whereas in the alkaline solutions, they dissolved through Reactions (12) and (13). The effect of the fluid-rock interaction was to drive the pH of the acidic and alkaline solutions to a value of ~5, which induced tungsten mineral precipitation.

$$CaWO_4 + OH^- = WO_4^{2-} + CaOH^+ \quad (12)$$

$$FeWO_4 + 3OH^- = WO_4^{2-} + HFeO_2^- + H_2O \quad (13)$$

4.2.4. Calcium and iron concentration

Several studies have proposed that fluid mixing is important for tungsten ore-formation as this process introduces Ca^{2+} and Fe^{2+} into the hydrothermal ore fluid, which commonly has very low concentrations of these cations because of its exsolution from a highly fractionated S-type granitic magma (Lecumberri-Sanchez et al., 2017; Yang et al., 2019). To test the fluid-mixing hypothesis, we modeled the mixing of a high salinity, tungsten-saturated brine, containing no Ca^{2+} and Fe^{2+}, with a low salinity, tungsten-free fluid containing Ca^{2+} or Fe^{2+} at 400 °C and 1000 bar (Fig. 11(a and b)). The former brine represents the hydrothermal fluid originating from the granitic magma, and the latter brine a formational water. The results of the modeling show that scheelite and ferberite precipitate strongly in response to increased concentrations of calcium and iron via Reaction (14).

$$H_mWO_4^{(m-2)} + MCl_n^{(2-n)} = MWO_4 + mH^+ + nCl^- \quad (14)$$

$$M = Fe^{2+} \text{ or } Ca^{2+}; \quad m = 0 \text{ or } 1 \text{ or } 2; \quad n = 0 \text{ to } 2 \text{ or } 4$$

In short, a hot, very acidic or alkaline saline hydrothermal fluid with low concentrations of Ca and Fe has a high capacity to transport tungsten. Tungsten mineral precipitation, on the other hand is favored by low temperature, near neutral pH and high concentrations of Ca and Fe.

5. CONCLUSIONS

The results of this study show that tungsten is dissolved in NaCl-bearing fluids as $H_2WO_4^0$ at low pH and HWO_4^- at moderately acidic to near-neutral pH. Contrary to the conclusion of some earlier studies, $NaHWO_4^0$ and $NaWO_4^-$ do not play a role in tungsten transport. The distribution of tungsten species is therefore controlled mainly by pH, and salinity promotes dissolution of tungsten minerals by increasing the ionic strength of the solution. The geological modeling in this paper suggests that a hot, saline, acidic or alkaline hydrothermal fluid with low concentrations of calcium and iron is an ideal ore-fluid for tungsten.

ACKNOWLEDGEMENTS

The experimental work in this paper was carried out in the Fluid-Rock Interaction Laboratory, Department of Earth and Planetary Sciences, McGill University and was funded by the

Strategic Priority Research Program (B) of the Chinese Academy of Sciences (XDB18000000); a NSERC Discovery grant to AEW-J; the National Natural Science Foundation of China (41603052; 41673067); the National Key Research and Development Program of China (2016YFC0600204); and a Chinese Government Scholarship from the China Scholarship Council. We thank Anna Katharina Jung for her assistance in conducting the ICP-MS analyses, and Caroline Seyler for her assistance in conducting the XRD analyses. Discussions with Olga Vasyukova, Yuan Mei, Jethro Sanz-Robinson, and Jiaxin Wang helped improve the manuscript. We are grateful for the constructive reviews of George Dan Miron, Joel Brugger, and an anonymous referee that improved this manuscript significantly, and the editorial assistance and comments of Editor Zoltan Zajacz and Jeffrey G. Catalano.

APPENDIX. SUPPLEMENTARY MATERIAL

Supplementary data to this article can be found online at https://doi.org/10.1016/j.gca.2019.09.013.

REFERENCES

Bailly L., Grancea L. and Kouzmanov K. (2002) Infrared microthermometry and chemistry of wolframite from the Baia Sprie epithermal deposit, Romania. *Econ. Geol.* **97**, 415–423.

Campbell A., Rye D. and Petersen U. (1984) A hydrogen and oxygen isotope study of the San Cristobal Mine, peru – implications of the role of water to rock ratio for the genesis of wolframite deposits. *Econ. Geol.* **79**, 1818–1832.

Campbell A. R. and Robinsoncook S. (1987) Infrared fluid inclusion microthermometry on coexisting wolframite and quartz. *Econ. Geol.* **82**, 1640–1645.

Gibert F., Moine B., Schott J. and Dandurand J. L. (1992) Modeling of the transport and deposition of tungsten in the scheelite-bearing calc-silicate gneisses of the montagne noire, France. *Contrib. Mineral. Petrol.* **112**, 371–384.

Heinrich C. A. (1990) The chemistry of hydrothermal tin(-tungsten) ore deposition. *Econ. Geol.* **85**, 457–481.

Helgeson H. C. and Kirkham D. H. (1974) Theoretical prediction of the thermodynamic behavior of aqueous electrolytes at high pressures and temperatures; I, Summary of the thermodynamic/electrostatic properties of the solvent. *Am. J. Sci.* **274**, 1089–1198.

Helgeson H. C., Kirkham D. H. and Flowers G. C. (1981) Theoretical prediction of the thermodynamic behavior of aqueous electrolytes by high pressures and temperatures; IV, Calculation of activity coefficients, osmotic coefficients, and apparent molal and standard and relative partial molal properties to 600 degrees C and 5kb. *Am. J. Sci.* **281**, 1249–1516.

Holland T. J. B. and Powell R. (1998) An internally consistent thermodynamic data set for phases of petrological interest. *J. Metamorph. Geol.* **16**, 309–343.

Johnson J. W., Oelkers E. H. and Helgeson H. C. (1992) SUPCRT92: A software package for calculating the standard molal thermodynamic properties of minerals, gases, aqueous species, and reactions from 1 to 5000 bar and 0 to 1000°C. *Comput. Geosci.* **18**, 899–947.

Keppler H. and Wyllie P. J. (1991) Partitioning of Cu, Sn, Mo, W, U, and Th between melt and aqueous fluid in the systems haplogranite-H_2O–HCl and haplogranite-H_2O–HF. *Contrib. Mineral. Petrol.* **109**, 139–150.

Kestin J., Sengers J. V., Kamgar-Parsi B. and Sengers J. M. H. L. (1984) Thermophysical properties of fluid H_2O. *J. Phys. Chem. Ref. Data* **13**, 175–183.

Korges M., Weis P., Lüders V. and Laurent O. (2018) Depressurization and boiling of a single magmatic fluid as a mechanism for tin-tungsten deposit formation. *Geology* **46**, 75–78.

Lecumberri-Sanchez P., Vieira R., Heinrich C. A., Pinto F. and Walle M. (2017) Fluid-rock interaction is decisive for the formation of tungsten deposits. *Geology* **45**, 579–582.

Lu H. Z., Liu Y. M., Wang C. L., Xu Y. Z. and Li H. Q. (2003) Mineralization and fluid inclusion study of the Shizhuyuan W-Sn-Bi-Mo-F skarn deposit, Hunan province, Cehina. *Econ. Geol.* **98**, 955–974.

Manning D. A. C. and Henderson P. (1984) The behavior of tungsten in granitic melt-vapor systems. *Contrib. Mineral. Petrol.* **86**, 286–293.

Marshall W. L. and Franck E. U. (1981) Ion product of water substance, 0–1000 °C, 1–10,000 bars new international formulation and its background. *J. Phys. Chem. Ref. Data* **10**, 295–304.

Mei Y., Sherman D., Liu W. and Brugger J. (2014) Metal complexation and ion hydration in low density hydrothermal fluids: ab initio molecular dynamics simulation of Cu(I) and Au (I) in chloride solutions (25–1000 °C, 1–5000 bar). *Geochim. Cosmochim. Acta* **131**, 196–212.

Mei Y., Sherman D., Liu W., Etschmann B., Testemale D. and Brugger J. (2015) Zinc complexation in chloride-rich hydrothermal fluids (25 to 600 °C): a thermodynamic model derived from ab initio molecular dynamics. *Geochim. Cosmochim. Acta* **150**, 265–284.

Migdisov A. A. and Williams-Jones A. E. (2007) An experimental study of the solubility and speciation of neodymium (III) fluoride in F-bearing aqueous solutions. *Geochim. Cosmochim. Acta* **71**, 3056–3069.

Minubaeva Z. (2007) *UV Spectroscopic Studies of the Hydrothermal Geochemistry of Molybdenum and Tungsten*. ETH Zurich.

Ni P., Wang X.-D., Wang G.-G., Huang J.-B., Pan J.-Y. and Wang T.-G. (2015) An infrared microthermometric study of fluid inclusions in coexisting quartz and wolframite from Late Mesozoic tungsten deposits in the Gannan metallogenic belt, South China. *Ore Geol. Rev.* **65**, 1062–1077.

Oelkers E. H. and Helgeson H. C. (1990) Triple-ion anions and polynuclear complexing in supercritical electrolyte solutions. *Geochim. Cosmochim. Acta* **54**, 727–738.

Oelkers E. H. and Helgeson H. C. (1991) Calculation of activity coefficients and degrees of formation of neutral ion pairs in supercritical electrolyte solutions. *Geochim. Cosmochim. Acta* **55**, 1235–1251.

Pankratz L. and Mrazek R. V. (1982) *Thermodynamic Properties of Elements and Oxides*. U.S. Bureau of Mines Bulletin, p. 672.

Polya D. A. (1988) Efficiency of hydrothermal ore formation and the Panasqueira W-Cu(Ag)–Sn vein deposit. *Nature* **333**, 838.

Polya D. A. (1989) Chemistry of the main-stage ore-forming fluids of the Panasqueira W-Cu(Ag)-Sn deposit, Portugal – Implications for models of ore genesis. *Econ. Geol.* **84**, 1134–1152.

Robie R. A. and Hemingway B. S. (1995) *Thermodynamic Properties of Minerals and Related Substances at 298.15 K and 1 bar (10^5 pascals) Pressure and at Higher Temperatures*. US Government Printing Office.

Romer R. L. and Lüders V. (2006) Direct dating of hydrothermal W mineralization: U-Pb age for hübnerite ($MnWO_4$), Sweet Home Mine, Colorado. *Geochim. Cosmochim. Acta* **70**, 4725–4733.

Ryzhenko B. N., Bryzgalin O. V., Artamkina I. Y., Spasennykh M. Y. and Shapkin A. I. (1985) An electrostatic model for the electrolytic dissociation of inorganic substances dissolved in water. *Geochem. Int.* **22**, 128–144.

Shock E. L., Sassani D. C., Willis M. and Sverjensky D. A. (1997) Inorganic species in geologic fluids: Correlations among stan-

dard molal thermodynamic properties of aqueous ions and hydroxide complexes. *Geochim. Cosmochim. Acta* **61**, 907–950.

Shvarov Y. (2015) A suite of programs, OptimA, OptimB, OptimC, and OptimS compatible with the Unitherm database, for deriving the thermodynamic properties of aqueous species from solubility, potentiometry and spectroscopy measurements. *Appl. Geochem.* **55**, 17–27.

Shvarov Y. V. and Bastrakov E. (1999) HCh: a software package for geochemical equilibrium modelling. *User's Guide*, 25.

Shvarov Y. V. (2008) HCh: New potentialities for the thermodynamic simulation of geochemical systems offered by windows. *Geochem. Int.* **46**, 834–839.

Sverjensky D. A., Shock E. L. and Helgeson H. C. (1997) Prediction of the thermodynamic properties of aqueous metal complexes to 1000°C and 5 kb. *Geochim. Cosmochim. Acta* **61**, 1359–1412.

Soloviev S. G. and Kryazhev S. G. (2017) Geology, mineralization, and fluid inclusion characteristics of the Skrytoe reduced-type W skarn and stockwork deposit, Sikhote-Alin, Russia. *Miner. Depos.* **52**, 903–928.

Tagirov B. R., Zotov A. V. and Akinfiev N. N. (1997) Experimental study of dissociation of HCl from 350 to 500°C and from 500 to 2500 bars: Thermodynamic properties of HCl° (aq). *Geochim. Cosmochim. Acta* **61**, 4267–4280.

Timofeev A., Migdisov A. A. and Williams-Jones A. E. (2017) An experimental study of the solubility and speciation of tantalum in fluoride-bearing aqueous solutions at elevated temperature. *Geochim. Cosmochim. Acta* **197**, 294–304.

Wei W., Hu R., Bi X., Peng J., Su W., Song S. and Shi S. (2012) Infrared microthermometric and stable isotopic study of fluid inclusions in wolframite at the Xihuashan tungsten deposit, Jiangxi province, China. *Miner. Depos.* **47**, 589–605.

Wesolowski D., Drummond S. E., Mesmer R. E. and Ohmoto H. (1984) Hydrolysis equilibria of tungsten(VI) in aqueous sodium-chloride solutions to 300-degrees-c. *Inorg. Chem.* **23**, 1120–1132.

Wood S. A. (1992) Experimental determination of the solubility of WO_3(s) and the thermodynamic properties of H_2WO_4(aq) in the range 300–600 C at 1 kbar: calculation of scheelite solubility. *Geochim. Cosmochim. Acta* **56**, 1827–1836.

Wood S. A. and Samson I. M. (2000) The hydrothermal geochemistry of tungsten in granitoid environments: I. Relative solubilities of ferberite and scheelite as a function of T, P, pH, and m_{NaCl}. *Econ. Geol.* **95**, 143–182.

Wood S. A. and Vlassopoulos D. (1989) Experimental determination of the hydrothermal solubility and speciation of tungsten at 500° C and 1 kbar1, 2. *Geochim. Cosmochim. Acta* **53**, 303–312.

Yang J.-H., Zhang Z., Peng J.-T., Liu L. and Leng C.-B. (2019) Metal source and wolframite precipitation process at the Xihuashan tungsten deposit, South China: Insights from mineralogy, fluid inclusion and stable isotope. *Ore Geol. Rev.* **111**, 102965.

Zhu Y.-N. and Peng J.-T. (2015) Infrared microthermometric and noble gas isotope study of fluid inclusions in ore minerals at the Woxi orogenic Au–Sb–W deposit, western Hunan, South China. *Ore Geol. Rev.* **65**(Part 1), 55–69.

Associate Editor: Zoltan Zajacz